Proceedings of ASME Turbo Expo 2011
GT2011
June 6-10, 2011, Vancouver, British Columbia, Canada

GT2011-46660

COAL ASH DEPOSITION ON NOZZLE GUIDE VANES: PART II - COMPUTATIONAL MODELING

B. Barker, B. Casaday, P. Shankara, A. Ameri, J. P. Bons
Department of Mechanical and Aerospace Engineering
Ohio State University
Columbus, OH 43235

ABSTRACT

Coal ash deposition was numerically modeled on a GE-E^3 high pressure turbine vane passage. A model was developed, in conjunction with Fluent™ software, to track individual particles through the turbine passage. Two sticking models were used to predict the rates of deposition which were subsequently compared to experimental trends. The strengths and limitations of the two sticking models, the critical viscosity model and the critical velocity model, are discussed. The former model ties deposition exclusively to particle temperature while the latter considers both the particle temperature and velocity. Both incorporate some level of empiricism, though the critical viscosity model has the potential to be more readily adaptable to different ash compositions. Experimental results show that both numerical models are reasonably accurate in predicting the initial stages of deposition. Beyond the initial stage of deposition, transient effects must be accounted for.

INTRODUCTION

Traditional petroleum based fuels are becoming less accepted due to political and environmental concerns. To help meet with the demand for energy, engineers are using fuels derived from alternative sources. The direct liquefaction and gasification of coal has provided an alternative fuel for turbine engines in power generators. Coal is widely available and is inexpensive compared to natural gas. Drawbacks to coal derived fuels, however, include negative impacts on the environment and more pollutants during combustion. Airborne particulates known as fly ash can deposit on the internal walls of the engine and degrade the system over time. Increased surface roughness resulting from such deposition augments the heat transfer from the high temperature fluid to the surfaces. Removal of the deposits is expensive and time consuming as the afflicted parts need to be removed for cleaning and repair. Understanding how the particulate adheres to the walls and under what conditions is crucial to reducing the amount of deposition. Reducing the deposition will reduce the time spent cleaning the engine and prolong the life of the hardware.

There have been many studies looking into the causes and effects of deposition on turbine hardware. Small-scale deposition can increase the surface roughness. Bons [1] concluded that increases in surface roughness can decrease turbine performance. Abuaf et. al. [2] supported the finding that losses are associated with increased roughness and found that the heat transfer was increased with additional roughness. Large-scale deposition was found to be even more damaging to turbine hardware. Kim et. al. [3] conducted experiments exploring the effects of volcanic ash on turbine hardware. They found that deposition can clog film cooling holes and can lead to failure of the turbine vanes. Dunn et. al. [4] also studied the effects of volcanic ash and found that damage due to deposition was related to the turbine inlet temperature, concentration of particulate and the material properties of the volcanic ash. Dunn et. al. confirmed that deposition can clog film cooling holes and that deposition is a major issue for modern engines with high combustor temperatures. Dunn et. al. also noted that aircraft engines that ingest particle laden flow have increased difficulty in restarting and that engines exposed to sufficient levels of particulate can be damaged beyond repair. Sundaram and Thole [5] studied the effects of deposition on film cooling and found that film cooling effectiveness degrades as deposition forms near and in film cooling holes. Lewis et. al. [6] found that the location of deposition around film cooling holes can affect the heat transfer. Deposition that forms between and downstream of film cooling holes causes the high temperature free stream to flow into the deposition valleys and increases heat transfer into the surface. Lawson et. al. [7] conducted experiments in a low speed wind tunnel using low melt wax to investigate the sticking mechanism and formation of deposits on a flat plate. Jensen et. al. [8] and Crosby et. al. [9] constructed the Turbine Accelerated Deposition Facility (TADF) and observed the growth of deposits on one inch coupons. This facility was operated at actual engine temperatures and used coal fly ash for particulate. Smith et. al. [10] constructed the Turbine Reaction Flow Rig (TuRFR) and tested actual turbine hardware at engine temperatures and velocities. Deposition from coal fly ash was found to form on the pressure surface and leading edge of the turbine vanes. The negative effects of deposition have demanded that the mechanisms of deposition formation be better understood yet the difficulties in operating experiments at engine operating conditions has supported the need for computer modeling of deposition.

Numerical models of deposition have been the focus of much exploration due to the freedoms of computational fluid dynamic research. Hossain et. al. [11] developed a model to track particles through piping with bends. They found that small diameter particles were less likely to deposit on the walls because they had a higher tendency to follow the flow. Larger particles with higher inertia were more likely to deposit downstream of the bends. Tabakoff et. al. [12] numerically and experimentally tracked ash particle trajectories through an axial turbine to predict erosion patterns. Longmire [13] looked into the particle trajectories and developed corrections for particle dispersion when predicting particle flow near surfaces. El-Batsh and Haselbacher [14] developed a sticking model to quantify the criteria for particle sticking and detachment. They tested a 2D turbine vane cascade to study the locations where deposition was most likely. Ai [15] modified the sticking model developed by El-Batsh and Haselbacher and calibrated it to match experimental results. Tafti et. al. [16] developed a sticking model using the coal ash composition to determine a sticking probability based on the viscosity-temperature relationship. The model from El-Batsh and Haselbacher modified by Ai is limited in that calibration is required for the model to match experimental results. Tafti et. al.'s model is limited in that it does not account for particulate removal or detachment. Validation of these models has been limited due to insufficient experimental data and neither model has been applied to deposition on real geometries found in turbo machinery with real ash properties.

The focus of the study presented in this paper is the implementation of these sticking models on a 3D turbine vane, and a comparison with experimental results to determine if deposition can be accurately modeled. The bulk of the experimental results are included in the Part I companion paper [17]. This study explores the 3D flow path effects on particle trajectories, as well as the capture efficiencies for particles of varying size. This study also discusses mechanisms for deposition accumulation and removal for transient studies.

METHODS

Ash particle deposition was numerically modeled on a GE-E^3 turbine vane geometry using the flow solver in Fluent and sticking models developed in C language incorporated as User Defined Functions (UDF) in Fluent. A depiction of the grid used for the solver is shown in Figure 1, containing 581512 total cells for a single vane passage. The computational domain extends 0.74 axial chord lengths upstream and 0.74 axial chord lengths downstream. The grid is refined near the walls and the y^+ value of the converged solution is below 0.5 at all wall locations, with an average y^+ value of 0.1. The grid was considered sufficiently refined after comparing the converged solution to an identical geometry with nearly double the number of cells, and the velocity field was identical to within 99% of the total flow rate.

In this study, the deposition model predictions are compared to experimental data obtained in the TuRFR, described in Part I [17]. Unfortunately, the turbine vanes studied experimentally in the TuRFR used CFM56 vanes and were not identical to the E^3 geometry used numerically. The CFM56 geometry would have been preferred in the numerical tests in order to better compare to the experimental results, but the CFM56 geometry was not available for computational study. Because the two vane geometries have similar chord lengths, solidities, flow turning angles, and aspect ratios, a qualitative comparison was assumed valid for the tests. Another difference between the experimental and computational geometry was the absence of film cooling holes in the E^3 geometry. Experiments reported in Part I showed that deposition tended to accumulate, at least initially, around film cooling holes on the CFM56 vanes. This is another mitigating factor in the validation with experimental results.

FLOW SOLVER

The particle trajectory modeling was done using the DPM module in FLUENT. The DPM uses an Euler-Lagrange approach to track the particle trajectories. The DPM module allows for flow induced forces to be computed as they determine the flow path of the particles. This method is described below.

The Eulerian-Lagrangian model splits the particulate modeling into two phases. The first phase (Eulerian) is generating the flow solution absent of particulate. The flow solution phase is treated as a continuum and the Navier-Stokes equations are solved throughout the fluid domain. The second phase is tracking a large number of dispersed particles traveling through the flow. The trajectory of each particle is predicted and stored for analysis. Zhang & Chen [18] found this method to provide accurate results that are easy to interpret but are computationally expensive.

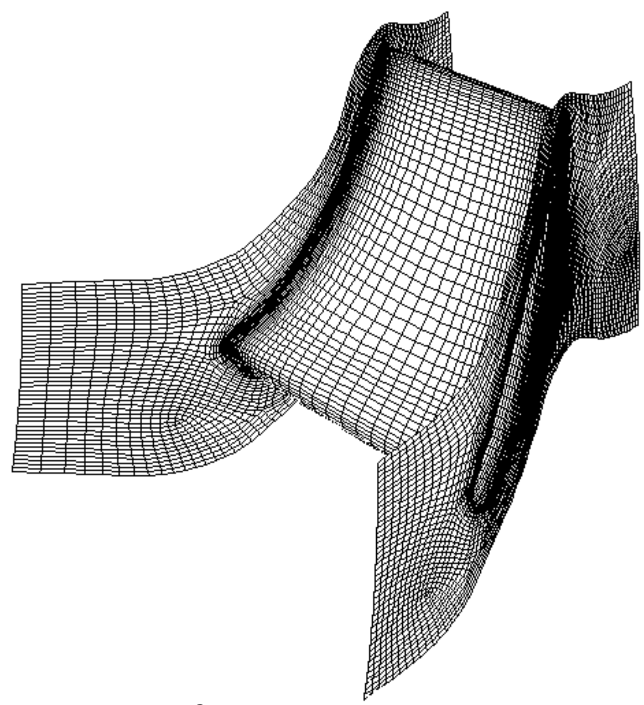

Figure 1 - GE-E^3 turbine vane grid used in Fluent flow solver.

Typically, the fraction of particles in an engine is around 0.1 parts per million by weight (ppmw) [19]. Coal fly ash particulate has a much higher density than the fluid and the number of particles is low enough for inter-particle collisions to be neglected. Kulick et. al. [20] and Kaftori et. al. [21] have shown that for volume fractions less than 10E-6 the turbulence modification due to particles in the flow is negligible. For these reasons, particles are assumed to have no effect on the fluid flow or trajectory of other particles.

The TuRFR experimental tests presented in Part I augmented the particulate injected to accelerate deposition, but the volume fraction remained well below 10E-6, typically between 1.3E-7 to 3E-7, so that the particulate is assumed to have no effect on the flow field.

The governing equations that define the flow solution are the conservation of mass, momentum, and energy for compressible, turbulent flow. The turbulence modeling used was the k-ω model due to its preference over k-ε model for non-zero pressure gradients.

The boundary conditions required for the solution are set static pressure and temperature at the inlet, static pressure at the outlet, and no slip at the walls. A circumferential periodic boundary condition is used to simulate an entire vane passage ring from an individual vane geometry. This periodic condition accounts for 46 vanes in the entire passage.

The flow solution was considered converged when residuals decreased more than four orders of magnitude and oscillations in the total flow rate were less than 0.1% of the absolute magnitude across iterations.

After the flow solution was accurately converged, ash particles were injected into the domain and tracked using the Discrete Phase Model (DPM) module in Fluent. The particles in this study were injected at specified locations across the inlet boundary as shown in Figure 2. There are 900 injection points located at 30 radial positions and 30 angular positions. Particles were assumed to be in thermal equilibrium with the flow at the inlet and were injected at the local flow velocity and direction. Each injection point injected one particle at a time.

Fluent predicts the trajectory of a discrete phase particle by the balance of forces on the particle. The particle inertia is balanced with the forces acting on the particle. The turbulent dispersion of particles was modeled using stochastic tracking, also known as the random walk, in Fluent. For turbulent flows, the instantaneous random velocity, u', is used to predict the perturbation of the particle. Fluent calculates u' based on an isotropic turbulence assumption; however, this assumption is inaccurate in the viscous sub layer. Dehbi [22] developed relations for u' that correct for the non-isotropic behavior in this region. To avoid spurious behavior near the surface, the random walk feature was disabled within 200 y^+ distance to the surface.

In this study, the following assumptions were made regarding the interaction between the fluid phase and the particles. The particles are assumed to be perfect spheres that are considered as points located at the center of sphere. SEM (scanning electron microscope) images revealed that the ash particles used in the experimental studies were spherical in shape [23]. The various forces acting on the particle were described by Rudinger [24].The dominant force on the particles is the drag caused by the fluid flow. For small particles on the order of 1 μm diameter, the Saffman force is also significant, especially in shear regions near the wall boundaries, and for this reason, both forces are included in the model. Other forces, such as gravity, Brownian, Magnus, and rarefaction effect, were neglected due to negligible effects on particle sizes ranging from 1 μm to 100μm, which are the particle sizes of interest.

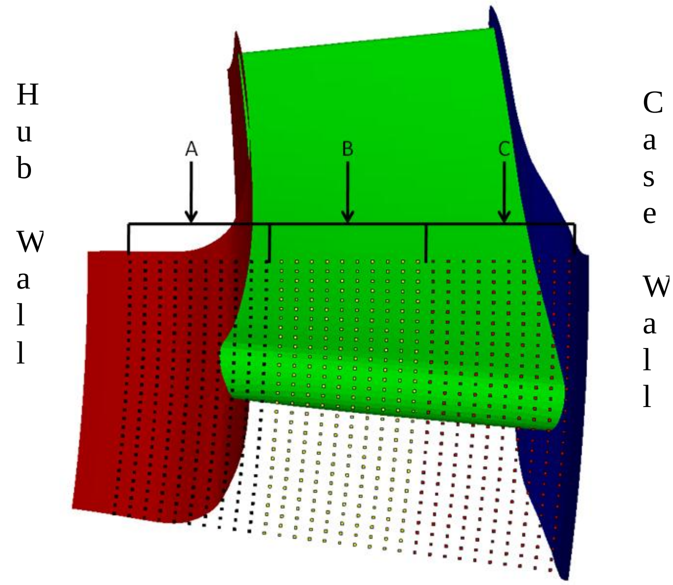

Figure 2 - Representation of injection point grid where ash particles were initially tracked.

When modeling deposition, it is useful to define three parameters to measure the performance of the simulations. The impact, sticking and capture efficiencies are defined below.

$$Impact\ \% = \frac{Mass\ of\ particulate\ impacting\ surface}{Total\ mass\ of\ particulate\ injected} \quad [1a]$$

$$Sticking\ \% = \frac{Mass\ of\ particulate\ sticking\ to\ surface}{Mass\ of\ particulate\ impacting\ surface} \quad [1b]$$

$$Capture\ \% = \frac{Mass\ of\ particulate\ sticking\ to\ surface}{Total\ mass\ of\ particulate\ injected} \quad [1c]$$

The impact efficiency is useful for measuring how likely particles are to hit the surface. Small particles are more likely to follow the flow and less likely to hit the surface, whereas larger particles, having more inertia, hit the surfaces more often. The impact efficiency is therefore higher for larger particles than smaller particles. The sticking efficiency shows how likely particles are to stick upon contacting the surface. The capture efficiency shows how much particulate of mass deposits on the surface relative to the mass injected. Based on these definitions, capture efficiency is equal to the product of the sticking efficiency and impact efficiency.

CRITICAL VISCOSITY MODEL

Tafti et. al. [16] developed a sticking model based on the particle viscosity. The particle viscosity changes with temperature and the relationship can be predicted based on the coal ash properties.

Tafti et. al. based their model on the probability of the particle sticking. The ash softening temperature is the critical sticking temperature, T_S. Particles above this temperature are assumed to have a sticking probability of one. Particles with temperature much less than the critical sticking temperature will have a sticking probability of zero. For particles with temperatures in-between, the probability function is found using:

$$P_S(T_P) = \frac{\mu_{crit}}{\mu_{T_P}} \quad [2]$$

where μ_{crit} is the viscosity of the particle at the critical sticking temperature and μ_{Tp} is the viscosity of the particle at the current particle temperature.

Senior and Srinivasachar [25] developed a method to determine the coal ash particle viscosity based on the coal ash chemical composition. N'Dala et. al. [26] have shown that the temperature dependence of viscosity of silicate and aluminosilicate melts can be described by:

$$\log\left(\frac{\mu}{T_P}\right) = A + \frac{10^3 B}{T_P} \quad [3]$$

where *A* and *B* are constants which depend on the chemical composition. Senior and Srinivasachar conducted experimental tests to develop a curve fit for determining *A* and *B*. The model is described in further detail in [25].

This model defined the sticking probability on the viscosity of the ash, but was limited in that it was not dependent on other parameters, such as particle impact velocity, particle mass, or angle of impact. It provided no mechanism for removal, and lacked experimental validation. It was also only usable for coal ash used in Senior and Srinivasachar's model, and not all ash compositions are compatible with this model.

CRITICAL VELOCITY MODEL

The critical velocity model uses the impact velocity component normal to the surface to determine if the particle sticks to the surface. The critical impact velocity is used as criterion for determining whether the particle sticks or reflects and is affected by various properties of the flow and particle. The critical velocity in this study is given as:

$$V_{cr} = \left[\frac{2E}{D_P}\right]^{\frac{10}{7}} \quad [4]$$

$$E = 0.51\left[\frac{5\pi^2(k_1+k_2)}{4\rho_P{}^{3/4}}\right]^{\frac{2}{5}} \quad [5]$$

$$k_1 = \frac{1-\nu_S^2}{\pi E_S} \quad [6]$$

$$k_2 = \frac{1-\nu_P^2}{\pi E_P} \quad [7]$$

where V_{cr} is the critical velocity, E is the composite Young's modulus, E_s is the surface Young's modulus, E_P is the Young's modulus of the particle, ν_s is the surface Poisson ratio and ν_P is the particle Poisson ratio. Particles that impact the surface with a normal velocity below the critical velocity will deposit. Those particles that impact with velocities above the critical impact velocity will reflect off the surface and continue their trajectory until they leave the domain or deposit on the surface further downstream.

The Young's modulus is sensitive to the temperature of the particle and can vary drastically at high temperatures. The material properties of the particle can also affect the Young's modulus. Due to the complications of measuring the Young's modulus for the particle, it is approximated using empirically derived functions. El-Batsh [28] developed a function of the Young's modulus to match his predicted capture efficiencies to experimental results. The function used by El-Batsh was:

$$E_P = 120(1589 - T_P)^3 \quad \text{for } T_p\text{>1100 K} \quad [8]$$

$$E_P = 3\times10^5(1589 - T_P) \quad \text{for } T_p\text{>1300 K} \quad [9]$$

Ai [15] developed a function for the particle Young's modulus based on coupon studies with coal ash. The function Ai used was:

$$E_P = 3\times10^{20} exp(-0.02365 T_g) \quad [10]$$

where T_g is the free stream gas temperature above the surface. Ai & Fletcher [23] made modifications to the function to include the surface temperature effects. The new correlation is:

$$E_P = 3\times10^{20} exp(-0.02365 T_{AVG}) \quad [11]$$

$$T_{AVG} = \frac{T_S+T_g}{2} \quad [12]$$

Another modification was made in this study to the function developed by Ai & Fletcher [27]; the temperature near the surface varies due to the thermal boundary layer. For flows where the surface is at a lower temperature than the free stream, the flow right above the surface will be lower temperature than the free stream. Depending on the thermal properties of the particle, the particle temperature may be at a higher temperature than the flow near the surface. For this study, T_{AVG} was modified by replacing the T_g in Eq. 12 with the particle temperature T_p, which is calculated in the particle tracking model.

PARTICULATE REMOVAL

Deposits can detach from the surface if the shear forces are sufficient to overcome the sticking force. Some particles may stick temporarily before being dislodged from the surface. The amount of deposit that is on the vane is determined by the balance of particles sticking and particles detaching.

Soltani & Ahmadi [29] studied different mechanisms for particle detachment and found that for spherical particles they are detached predominantly by rolling. Sliding and lifting are less important. Das et. al. [30] also found that rolling was the more dominant removal mechanism. El-Batsh [28] used this reasoning to develop a model for particle detachment, which is used as the detachment mechanism for the critical viscosity and critical velocity models in this study. Essentially, the local shear stress is calculated and compared to an estimated sticking force. More details are available in [28].

RESULTS

The flow solver was run with the same inflow condition measured in the experiment from Part I: inlet temperature = 1338K, inlet velocity = 64 m/s, and a pressure difference of about 85kPa. Figure 3 and Figure 4 show planar views of the flow solution at midspan. Figure 3 shows the fluid streamlines around the vane in two dimensions, as flow in the radial dimension is minimal. Figure 4 shows the local Mach number for the midspan. The flow solution was used to simulate the injection of thousands of ash particles, and either the critical viscosity model or critical velocity model was used to determine if the particles would deposit upon impacting the vane surface. The deposition removal scheme determined if any ash particles detached after sticking.

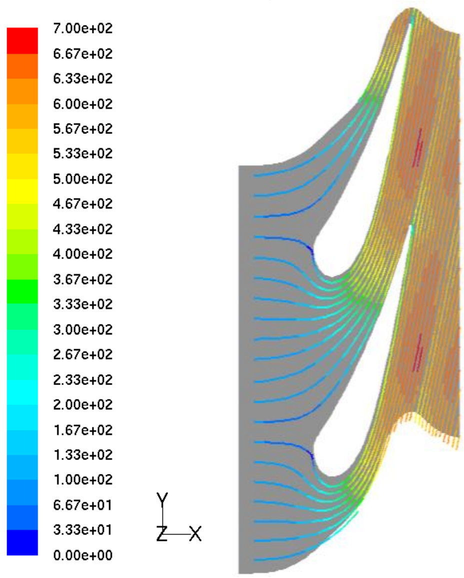

Figure 3 – Midspan view of fluid streamlines around vane surface. Colors represent velocity magnitude in m/s.

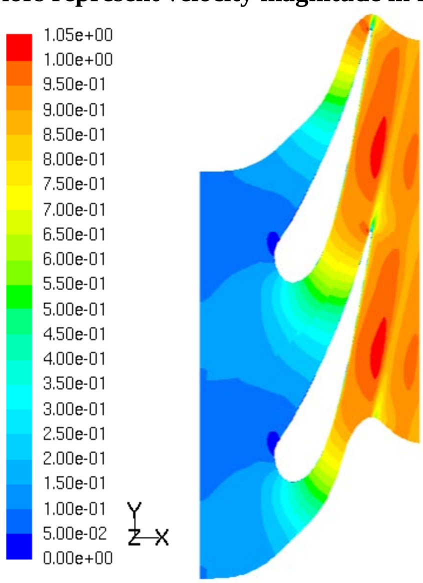

Figure 4 – Contours of local Mach number at geometry midspan.

PARTICLE IMPACT

Of the four ash samples used in Part I, this study focuses primarily on the JBPS subbituminous ash, with properties shown in Table 1. As mentioned in Part I, a Coulter Counter was used to measure the size distribution of this ash particulate (Figure 5). The particle sizes ranged from 1 μm or smaller up to about 40 μm.

Table 1 – JBPS Coal Ash Composition

Element Weight %									
SiO_2	CaO	Al_2O_3	Fe_2O_3	MgO	TiO_2	SrO	SO_3	K_2O	Na_2O
49.9	9.4	11.5	14.5	1.7	3.0	0.7	1.2	1.6	3.7

Bulk physical properties of the ash were assumed to be the same as those in [28]. The density of the particulate was estimated to be 1980 kg/m^3. The bulk ash density was measured as 990 kg/m^3 and a packing factor of 2.0 was assumed. The specific heat and thermal conductivity were assumed to be 984 J/kg-K and 0.5 W/m-K respectively.

For the critical viscosity model, the elemental composition in Table 1 was used to calculated the model coefficients, which were A = -11.31 and B = 15.96. The critical sticking temperature was assumed to be 1478 K, which was suggested by Vargas [31].

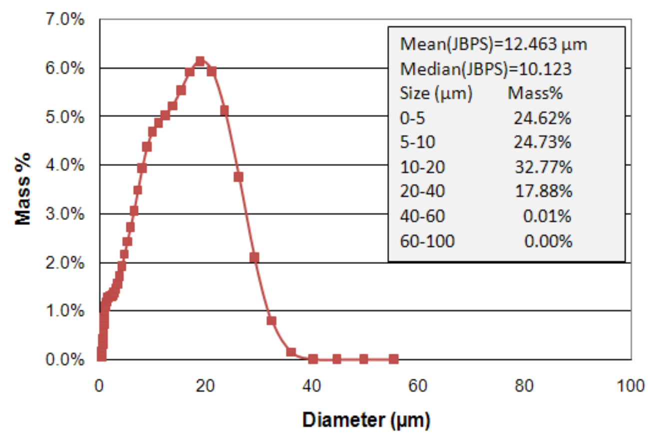

Figure 5 - Particle size distribution results from Coulter Counter for JBPS coal fly ash.

The flow solver simulated the injection of thousands of particles of various sizes to determine the relationship between particle size, impacts, and deposits. The particles were injected upstream of the vane and tracked until they exited the domain or attached to the surface. Figure 6 shows the potential path lines of three injected particles of different sizes all injected from the same point. The red line represents the largest particle with a 100 μm diameter. It does not follow the fluid streamlines and impacts both the leading edge of a vane and the pressure surface of an adjacent vane after rebounding. The green line represents a particle with a 10 μm diameter that impacts only the trailing edge of a vane. The blue line represents a particle with a 1 μm diameter. It closely follows the fluid streamlines (Figure 3) and never impacts the vane surface. All three particles were injected with a velocity and temperature identical to the fluid temperature and velocity at the injection site.

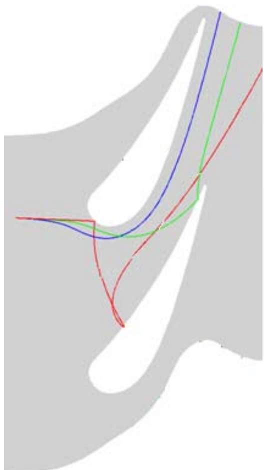

Figure 6 - Midspan view of path lines of three injected particles. Red = 100 μm diameter, Green = 10 μm diameter, and Blue = 1 μm diameter. No sticking model is incorporated.

The probability of a particle impacting the surface is dependent on the Stokes number of the particle, which is defined as:

$$St_k = \frac{\rho_p d_p^2 V_i}{18 \mu l_c} \qquad [13]$$

Where ρ_p is the particle density, d_p is the particle diameter, and μ is the fluid viscosity. V_i is a characteristic velocity and l_c is a characteristic length scale. For this study l_c is the leading edge diameter and V_i is the average axial velocity at the inlet of the vane geometry.

Larger Stokes number particles are less likely to be affected by the flow and more likely to impact the surface of the turbine vanes. Smaller Stokes number particles more closely follow the fluid streamlines shown in Figure 3 and were less likely to impact. Some particles impact the surface multiple times if they do not stick upon an initial impact. To illustrate this dependency on Stokes number, a test run was conducted that did not allow for multiple impacts. The impact efficiency is shown in Figure 7 for a range of Stokes numbers corresponding to diameters of 1 – 100 μm. The figure shows that all particles above a Stokes number of about 1.0, corresponding to a diameter of about 10 μm for the present flow conditions, impact the surface, and smaller particles experience a diminishing probability of impact. These test runs were conducted using the particle injection grid illustrated in Figure 2.

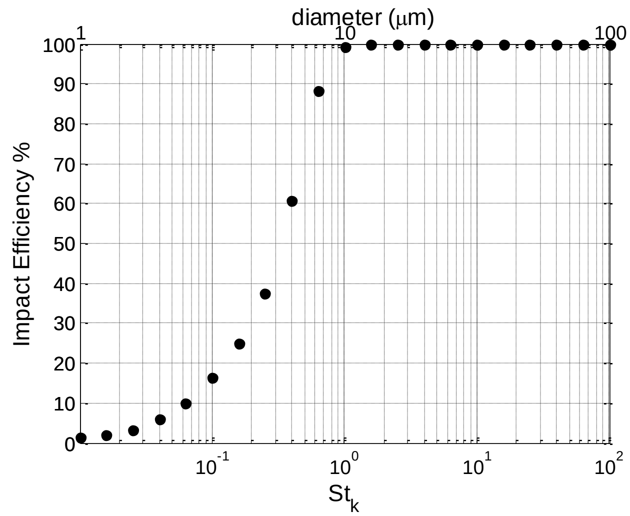

Figure 7 - Relationship between Stokes number and impact efficiency (Only single impacts are allowed – no rebound)

PARTICLE STICKING

The Stokes number has an indirect impact on particle sticking probabilities, according to the critical viscosity and critical velocity models. Ash particles were injected from the grid displayed in Figure 2 ranging in size from 1 μm to 100 μm, allowing for multiple impacts, and the sticking probabilities were recorded for each model. The results for impact efficiency and sticking efficiency are shown in Figure 8 and Figure 9, respectively. Figure 8 differs from Figure 7 only by allowing the particles to impact the vane surface multiple times if the particles do not stick. For both sticking models, particles larger than about 10 μm impacted the surface about 1 ½ times on average. One might expect the impact efficiency in Figure 8 to be identical for both models because the particle trajectories are calculated in the same manner, and indeed they are similar. The difference arises due to the difference in sticking efficiencies between the two models. Some particles will impact the surface multiple times in one model, but only impact once with the other model because the particle sticks upon the first impact.

Figure 9 illustrates that for the critical velocity model, the sticking probability is very dependent on the Stokes number. The particle sticks if its velocity normal to the surface is lower than a critical value, and it will reflect if the normal velocity is higher. Because smaller particles are less likely to strongly deviate from the fluid streamlines, it is expected that these particles will not only be less likely to impact the surfaces, but will also impact the surface at lower normal velocities when impacts do occur. Particles with a Stokes number below about 0.18 are nearly 100% likely to stick upon impacting according to the critical velocity model, and particles with a Stokes number above about 1.5 have nearly zero probability of sticking. Though Figure 9 suggests that there is a Stokes number threshold for sticking, it should be remembered that the critical velocity model is dependent on the normal impact velocity and Young's modulus, which is a function of temperature. The Stokes number sticking threshold will therefore change with different flow rates, operating temperatures, or Young's Modulus correlation to temperature (e.g. Eq. [11]).

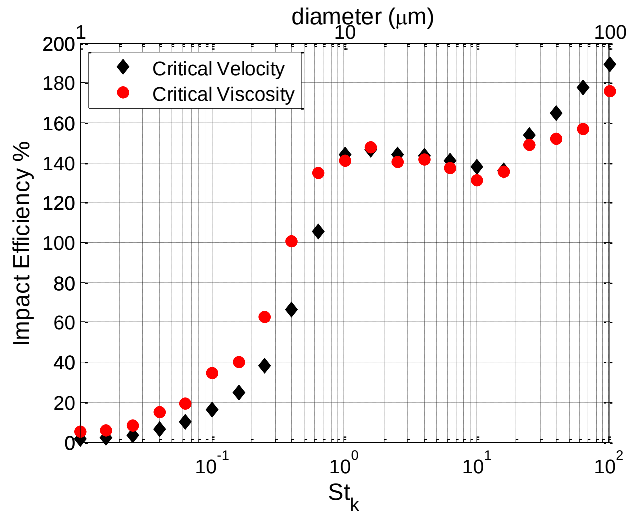

Figure 8 - Impact efficiency vs. Stokes number (particle diameter) for critical viscosity and critical velocity models. (Multiple impacts are allowed)

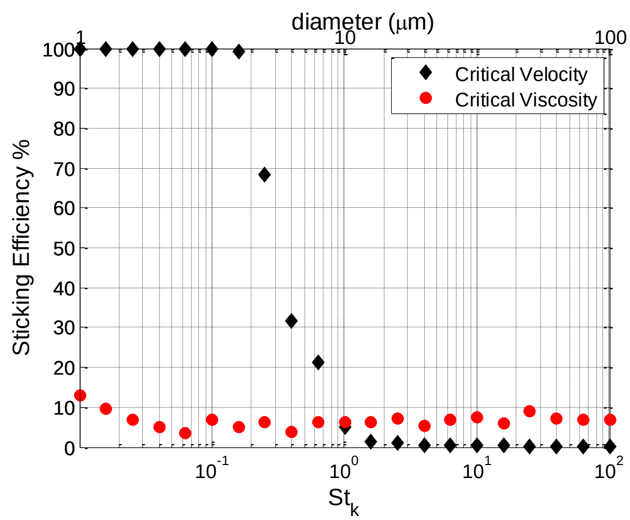

Figure 9 - Sticking efficiency vs. Stokes number (particle diameter) for critical viscosity and critical velocity models.

Alternatively, the sticking probability is relatively insensitive to Stokes number for the critical viscosity model. In this model, the sticking probability is only a function of temperature. The flow temperature changes about 100 deg C through the vane passage, but larger particles have greater thermal inertia and remain at a constant temperature longer than smaller particles. For this reason, the sticking probability is relatively constant across many orders of magnitude for the particle Stokes number, with slightly different probabilities for smaller particles. These particles have a slightly higher propensity to stick because they are heated while approaching the wall due to viscous heating near the adiabatic boundary. Both models account for the particle removal mechanism defined in the methods section, and a particle is only determined to stick if shear forces do not remove the particle from the surface.

PARTICLE CAPTURE

The capture efficiency is the product of the impact efficiency and sticking efficiency, giving the resultant deposition on the geometry. The relationship between capture efficiency and Stokes number are different for each sticking model, as shown in Figure 10. For the critical velocity model, the capture efficiency is large for a mid-range of particles, for large particles are not likely to stick and small particles are not likely to impact. For the critical viscosity model, the capture efficiency is lower for smaller particles yet higher for larger particles compared to the velocity model due to a more constant sticking probability. Interestingly, the capture efficiency is larger than the sticking efficiency for larger particles. This is because these particles impact the surface multiple times on average, bringing the impact efficiency above 100% (Figure 8).

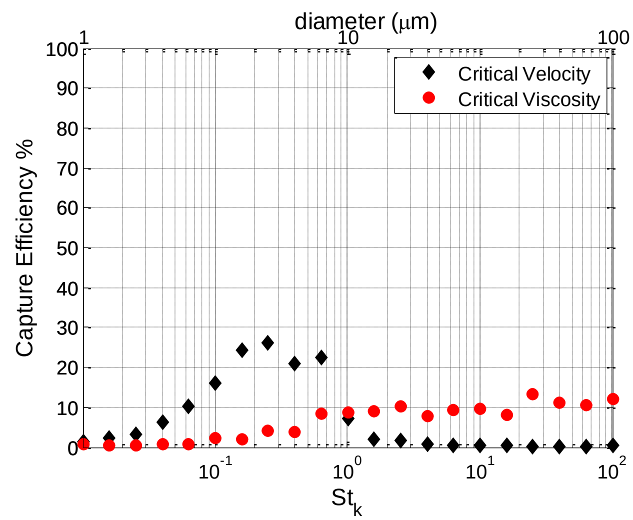

Figure 10 – Capture efficiency vs. Stokes number (particle diameter) for critical viscosity and critical velocity models.

To predict deposition on the E^3 geometry, a test was run with a distribution of particle diameters between 5 and 15 μm (ranging in Stoke's number from 0.25 to 2.3 and a mass averaged Stokes number of 1.0). This range was chosen to match the mass averaged Stokes number from the experimental tests[17]. Because the test injected multiples of 900 particles of each size (from each injection point), the range was restricted to 5 – 15 μm to conserve computational time. The results are shown in Table 2.

Table 2

	Total Injected #	Impact Efficiency %	Sticking Efficiency %	Capture Efficiency %
Critical Velocity Model	**18900**	**112**	**10.6**	**12.0**
Critical Viscosity Model	**18900**	**124**	**6.2**	**7.7**

Figure 11 and Figure 12 show the deposit locations on the vanes for the two models. Both models, although predicting different amounts of total deposition, predicted deposition in the same approximate areas of the vane. A majority of the particulate (~70%) deposited on the trailing half of the pressure side using the critical viscosity model, with less deposit on the leading edge. The critical velocity model predicted the deposit concentrated at the center of the pressure surface. For both models, no particulate deposited on the suction side of the vane, aside from near the leading edge, as no particles in this size range ever impacted the suction surface. The particulate was also slightly biased toward the hub endwall of the vane.

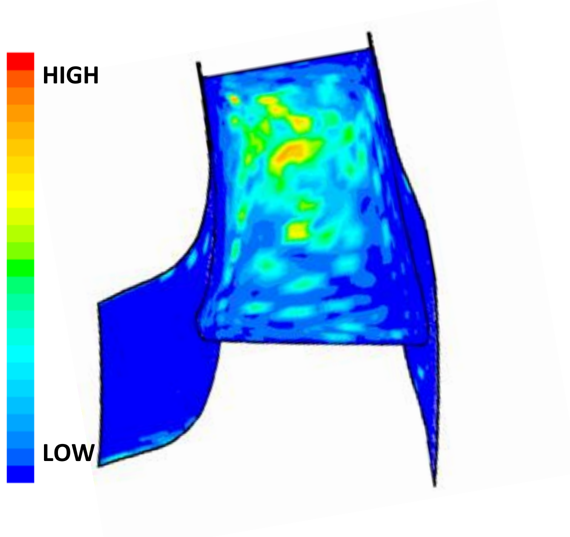

Figure 11 - Deposition concentration using critical viscosity model.

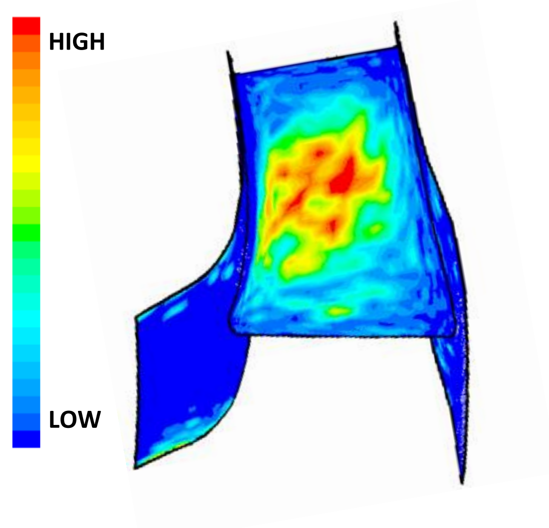

Figure 12 – Deposition concentration using critical velocity model.

For the critical viscosity, Tafti et. al.'s [16] model and Senior and Srinivasachar's [25] model were used to determine the viscosity of the ash. The critical sticking temperature was assumed to be 1478K. The table shows that the impact efficiency was higher for the critical velocity model compared to the viscosity model. Because the sticking model does not affect the path lines of the particles, one might expect the impact efficiencies to be identical for this test. However, if the sticking efficiency is higher for one model compared to another, particles that stick are limited to only one impact whereas they may otherwise impact the surface multiple times, as occurred in this case.

Additional tests were run with the critical viscosity model using the four different ash compositions studied experimentally in Part I [17]. Senior and Srinivasachar's model was used to acquire appropriate constants *A* and *B* for each ash except for the bituminous coal ash. The constants for this ash could not be calculated due to an iron content that exceeded the range stipulated by the model. Thus it was assumed to have the same constants as the JBPS ash. The values of *A* ranged from -11.32 to -9.61 and the values of *B* ranged from 10.66 to 15.98 for the three ash types. The relative ash densities were measured and the critical sticking temperature was initially assumed identical for all four ashes. Despite differences in particle density and composition [17], the results of these simulations were all very similar for the same Stokes number of the particles. The capture efficiency of the bituminous ash was approx. 8.2% (compared to 7.7% for the JBPS ash), and the capture efficiencies of the Lignite and PRB ashes were 6.8% and 6.2%, respectively. However, experimental results showed that the different ash types all had very different propensities to deposit. For the same particle loading, Lignite deposits were roughly 20% greater than JBPS, twice as thick as the PRB and more than 50 times greater than bituminous ash. This indicates that the constants *A* and *B* from Senior and Srinivasachar's model are not sufficient in distinguishing between deposition from different types or ranks of ash.

Much more significant than the *A* and *B* constants on the deposition of the critical viscosity model prediction is the critical sticking temperature. For example, a decrease in T_s of 50 deg C increases the capture efficiency from 7.7% to 16.7% for the JBPS ash. Numerous models have been created to try to predict the sticking temperature of ash based on chemical composition, (Lloyd et. al. [32], Seggiani [33]), but are not robust for different ash types. Four different regression equations provided by Lloyd et. al. were used to predict the sticking temperatures of the ash types used experimentally, but each equation provided very different temperatures and some were outside of the practical range (difference of 1000K for same ash composition). Sreedharan and Tafti [34] used a model developed by Yin et. al. [35] to predict the critical sticking temperatures for the eight ash types used in their tests. When applied to the four ash types used here, this model predicted the critical sticking temperature of the JBPS ash to be 1470 K, very similar to the assumed value of 1478 K. However, the model predicted the critical sticking temperatures of the other ash types to be below 1310 K, resulting in nearly 100% sticking efficiencies for these ash types. This unrealistic result highlights an area of critical need for future research in order to accurately implement the critical viscosity model.

COMPARISON WITH EXPERIMENTAL RESULTS

Experiments were run in the TuRFR to simulate the coal ash deposition of four different ash types discussed in detail in [17]. Tests were run where the ash particulate deposited on a CFM56 vane passage with or without film cooling. Because the computational model does not currently account for film cooling, the results from only the non-film cooling tests will be discussed. Based on these experimental tests, the Part I study made the following conclusions about the growth and formation of ash deposit.

- The ash was more likely to deposit with increased temperatures, but different ash types had different threshold temperatures for deposition. The hierarchy of deposition (from highest to lowest propensity) was: Lignite, JBPS, PRB, and Bituminous.
- The particles initially deposited in the film cooling holes on the pressure surface of the vanes near mid-chord. The deposits then proceeded to accumulate on and around other deposits, indicating that the ash is more likely to stick to pre-existing deposit.
- After the initial stages of deposition, more particulate accumulates on the leading edge, where the particulate eventually becomes the thickest.
- The particulate growth may become large relative to the thickness of the vane, significantly affecting the fluid flow through the vane passage.
- Deposit thickness is small at the trailing edge of the pressure surface.
- Particulate deposited only on the initial 18% of the wetted distance of the suction surface of the vane.
- Large-scale ash deposits could be removed from the surface, presumably due to shearing forces.

A sample test result reproduced from Part I is shown in Figure 13. It shows large ash structures that completely cover the pressure surface of the vane, with thickest deposit at the leading edge and thinner deposit at the trailing edge.

Figure 13 - JBPS Fly ash ~1050°C Post Test

Though the model predictions in Figure 11 and Figure 12 do not resemble the final experimental result in Figure 13, the computational model does agree with the initial stages of experimental deposition, as shown in Figure 14. This video still was taken early in the deposition test for sub-bituminous ash at an average temperature of 1080 deg C. The image shows deposits primarily near mid-chord on the pressure surface, with a slight propensity to the hub endwall, just like the model predicts. Apparently, once these initial deposits form, they have a first order effect on subsequent deposition through the altered surface curvature and modified impact probability.

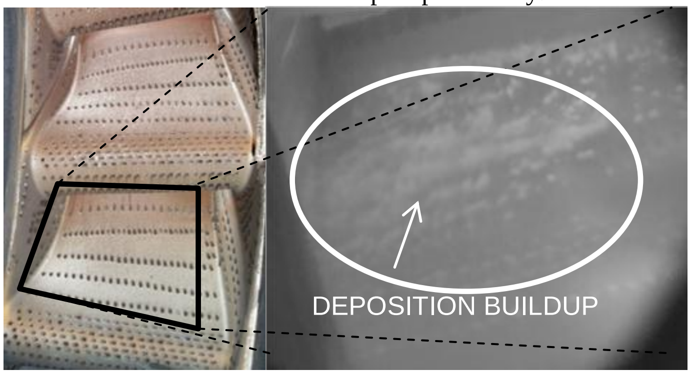

Figure 14 – Right image shows initial formation of ash deposition in experimental test. Left image shows clean vanes for spatial reference.

Experimental results showed large-scale deposit built up along the entire length of the pressure surface, except for a small length of the trailing edge (Figure 15). Interestingly, the large-scale deposition buildup is closely correlated to the Mach number (Figure 4) around mid-span. Though Fig. 4 is for the E^3 geometry, it is expected that the CFM56 vanes used in the experimental study of Part I will have similar nozzle Mach contours so a qualitative comparison is valid. Higher Mach numbers result in higher shear, which prevents deposit from building. Figure 15 illustrates that deposition is thick everywhere on the pressure surface except at the trailing edge. This thick deposit occurs where the Mach number is lowest, especially below Ma = 0.7. Deposits were also reduced (or absent entirely) on the suction surface, another high Mach number region.

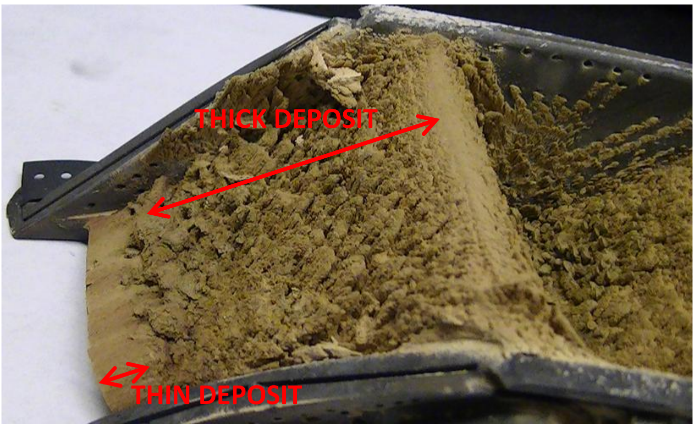

Figure 15 – Lignite Fly ash ~1050°C Post Test

CONCLUSIONS

The flow solver accurately predicts the trajectories and impact locations of ash particles prior to large-scale buildup of deposition. Both models predict deposition in the same general locations of the E^3 geometry, on the pressure side of the vane and slightly favored toward the hub endwall, in agreement with experimental observations of the initial stage of deposition. The critical viscosity model predicts the most deposit on the trailing half of the pressure side while the critical velocity model predicts deposition at mid-chord. Both the critical viscosity model and critical velocity model account for dynamic sticking probabilities of the particles upon impact. The critical viscosity model [21] has the capability to adjust the sticking probability for changes in temperature and ash composition, so the critical viscosity model may be preferred for comparing deposition rates of the different ash types used in the experimental study. However, this model requires that the critical sticking temperature be known which varies by ash type. Senior and Srinivasachar's model [21] predicts a viscosity based on temperature, but does not predict a critical sticking temperature. The constants A and B do not significantly change the results without a change in the critical sticking temperature, which is difficult to predict as evidenced by the results presented in this study.

The critical velocity model predicts the range of ash sizes that are likely to deposit. Unlike the critical viscosity model, the predicted range is also dependent on the velocity in addition to the temperature of the particle as it impacts the surface. For the present case, it predicted a larger capture efficiency than the critical viscosity model. This result is also dependent on the assumed dependency of Young's Modulus on temperature, which requires an empirically based correlation. Thus, both models have fundamental weaknesses that must be resolved by further research.

Even with a correct calibration for Young's Modulus or sticking temperature, the deposition models are only valid for the initial stages of deposition. After deposition has begun to form, transient effects become important and change the deposition process.

Despite the model not being able to accurately predict large-scale deposition, the numerical model is beneficial in predicting which particles will likely impact the surface with the potential for sticking. By filtering particles above a certain size, the number of particle impacts can be reduced to a point where deposition is significantly reduced. Results showed that most all particles with a Stokes number above 1.0 would impact the surface at least once for the given flow conditions. Alternatively, fewer than half of the particles with a Stokes number below 0.3 would impact the surface, and Stokes numbers below 0.05 would almost never impact. If deposition is prevented from ever building, then transient effects are not important and the model is valid.

ACKNOWLEDGEMENTS

The authors would like to express appreciation to Drs. Thomas Fletcher, Weiguo Ai, and Danesh Tafti for helpful discussions in the implementation of their models. This work was sponsored by a grant from the US Department of Energy and The Ohio State University Department of Mechanical and Aerospace Engineering. The views expressed in the article are those of the authors and do not reflect the official policy or position of the Department of Energy or U.S. Government.

NOMENCLATURE

A	Coefficient for critical viscosity model
B	Coefficient for critical viscosity model
D_P	Particle diameter
E	Composite Young's modulus
E_P	Young's modulus of particle
E_S	Young's modulus of surface
l_c	Chord length at midspan
T_P	Particle temperature
T_S	Critical sticking temperature
P_S	Probability of particle sticking
St_k	Stokes number
T_g	Free stream gas temperature
u'	Perturbation velocity
V_{crit}	Critical Velocity
V_i	Vane inlet velocity
X	Axial grid dimension
Y	Pitchwise grid dimension
Z	Spanwise grid dimension
ρ_p	Density of particle
μ_{crit}	Critical sticking viscosity
μ_{Tp}	Ash particle viscosity
ν_s	Surface Poisson ratio
ν_p	Particle Poisson ratio

REFERENCES

[1] Bons, Jeffrey P. "A Review of Surface Roughness Effects in Gas Turbines." *J. Turbomachinery,* Vol. 132, 021004 (2010).

[2] Abuaf, N., Bunker, R.S., Lee, C.P., "Effects of Surface Roughness on Heat Transfer and Aerodynamic Performance of Turbine Airfoils," *J. Turbomachinery,* Vol. 120, July 1998, pp 522-529.

[3] Kim, J., Dunn, M.G., and Baran, A.J. et al, "Deposition of Volcanic Materials in the Hot Sections of Two Gas Turbine Engines," *J. Engr. Gas Turbines & Power*, Vol. 115, Jul 1993, pp 641-651.

[4] Dunn, M. G., A. J. Baran, and J. Miatech. "Operation of Gas Turbine Engines in Volcanic Ash Clouds." *J.Eng. Gas Turbines and Power*, Vol. 118 pp. 724-731 (1996).

[5] Sundaram, N., Thole, K., "Effects of Surface Deposition, Hole Blockage, and Thermal Barrier Coating Spallation on Vane Endwall Film Cooling," *J. Turbomachinery.* Vol 129, July 2007, pp 599-607.

[6] Lewis, S., Barker, B., Bons, J.P., Ai, W., and Fletcher, T.H. "Film Cooling Effectiveness and Heat Transfer Near Deposit-Laden Film Holes." GT2009-59567. Presented at the IGTI 2009 conference and recommended for publication in the Journal of Turbomachinery publication, 2009

[7] Lawson, S.A., Thole, K., "The Effects of Simulated Particle Deposition on Film Cooling," presented at ASME Turbo Expo: Power for Land, Sea, and Air. June 8-12, 2009, Orlando, Florida USA. Paper #: GT2009-59109.

[8] Jensen, J.W., Squire, S.W., Bons, J.P., Fletcher, T.H., "Simulated Land-Based Turbine Deposits Generated in an Accelerated Deposition Facility," *J. Turbomachinery*. Vol. 127, July 2005, pp 462-470.

[9] Crosby, J.M., Lewis, S., Bons, J.P, Ai, W., Fletcher, T.H., "Effects of Particle Size, Gas Temperature, and Metal Temperature on high Pressure Turbine Deposition in Land Based Gas Turbines from Various Synfuels," presented at ASME Turbo Expo 2007: Power for Land, Sea, and Air. May 14-17, 2007, Montreal, Canada. Paper #: GT2007-25731.

[10] Smith, C., Barker, B., Clum, C., Bons, J.P. "Deposition in a Turbine Cascade with Combusting Flow."Presented at the ASME Turbo Expo 2010: Power for Land, Sea, and Air (2010)

[11] Hossain, A., and J. Naser. "CFD Investigation of Particle Deposition around Bend Ina Turbulent Flow." *15th Australasian Fluid Mechanics Conference* (2004).

[12] W. Tabakoff, A. Hamed, and M. Metwally. "Effect of Particle Size Distribution on Particle Dynamics and Blade Erosion in Axial Flow Turbines." J. Eng. Gas Turbines Power (1991) Vol. 113, Issue 4, 607

[13] Longmire, Pamela. "Computational Fluid Dynamics (CFD) Simulations of Aerosol in a U-Shaped Steam Generator Tube." Thesis. Texas A&M University, 2007.

[14] El-Batsh, H. and H. Haselbacher, "Numerical Investigation of the Effect of Ash Particle Deposition on the Flow Field through Turbine Cascades," IGTI, Amsterdam, Netherlands, GT-2002-30600 (2002).

[15] Ai, Weiguo. "Deposition of Particulate from Coal-Derived Syngas on Gas Turbine Blades Near Film Cooling Holes." Thesis. Brigham Young University, 2009.

[16] Tafti, Danesh K., and Sreedharan, S.S., "Composition Dependent Model for the Prediction of Syngas Ash Deposition with the Application to a Leading Edge Turbine Vane." *ASME Turbo Expo 2010: Power for Land, Sea, and Air* (2010).

[17] Webb, J., Casaday, B., Barker, B., Bons, J. P., Gledhill, A. D., Padture, N. P., "Coal Ash Deposition on Nozzle Guide Vanes: Part I – Experimental Characteristics of Four Coal Ash Types" Accepted for presentation at the ASME Turbo Expo 2011: Power for Land, Sea, and Air. June 14-18 Vancouver, Canada, GT2011-45894

[18] Zhang Z, Chen Q. "Comparison of the Eulerian and Lagrangian methods for predicting particle transport in enclosed spaces." *Atmospheric Environment* 2007; 41(25):5236-5248

[19] Wilcox, D.C. *Turbulence Modeling for CFD*, La Cañada, CA DCW Industries (1993)

[20] Kulick, J.D., Fessler, J.R., and Eaton, J.K., "Particle response and turbulence modification in fully developed channel flow", *J. Fluid Mech*., 277, 109-134, 1994

[21] Kaftori, D., Hetsroni, G., and Banerjee, S., "Particle behavior in the turbulent boundary layer. I. Motion, deposition, and entrainment", Phys. Fluids 7, 1095-1106, 1995

[22] Dehbi. A, A CFD model for particle dispersion in turbulent boundary layer flows, *Nucl. Eng. Des.* 238 (2008), pp. 707–715

[23] Bons, J. P., Crosby, J., Wammack, J.E., Bentley, B.I., and Fletcher, T.H., "High Pressure Turbine Deposition in Land-Based Gas Turbines with Various Synfuels," *ASME Journal of Engineering for Gas Turbines and Power*, Vol. 129, January 2007, pp. 135-143..

[24] Rudinger, G., "Fundamentals of gas-particle flow", Elsevier Scientific Pub. Co., Amsterdam, New York, 1980

[25] Senior, C. L., and Srinivasachar, S., "Viscosity of Ash Particles in Combustion Systems for Prediction of Particle Sticking." *Energy and Fuels* (1995).

[26] N'Dala, I.; Cambier, F.; Anseau, M. R.; Urbain, G. Viscosity of Liquid Feldspars. Part I: Viscosity Measurements.*Br. Ceram. Trans. J.* 1984,83, 108-112.

[27] Ai, W., Fletcher, T.H., "Computational Analysis of Conjugate Heat Transfer and Particulate Deposition on a High Pressure Turbine Vane," presented at ASME Turbo Expo 2009: Power for Land, Sea, and Air. June, 2009, Florida, United States. Paper #: GT2009-59573.

[28] El-Batsh, Hersham. "Modeling Particle Deposition on Compressor and Turbine Blade Surfaces." Thesis. Vienna University of Technology, 2001.

[29] Soltani, M., Ahmadi, G., "On particle adhesion and removal mechanisms." *Journal of Adhesion Science and Technology*, 1994. Vol. 8, No. 7, pp-763-785 (1994)

[30] Das, S. K.; Sharma, M. K. and Schechter, R. S. (1995), Adhesion and Hydrodynamic Removal of Colloidal Particles from Surfaces, Particulate Science and Technology, Vol.13, No. 3-4, pp. 227-247.

[31] Vargas, Signe. "Straw and Coal Ash Rheology." Thesis. Technical University of Denmark, 2001.

[32] Lloyd, Riley, Risen, Gilleland, Tibbitts, "Estimation of Ash Softening Temperatures Using Cross Terms and Partial Factor Analysis." *Energy and Fuels* (1990) 4, 360-364

[33] Seggiani, M., "Empirical correlations of the ash fusion temperatures and temperature of critical viscosity for coal and biomass ashes." Fuel 78 (1999) 1121-1125

[34] Sreedharan, S. S. and Tafti, D., "Composition dependent model for the prediction of syngas ash deposition in turbine gas hotpath." *Int. Journal of Heat and Fluid Flow* (2010) doi:10.1016/j.ijheatfluidflow.2010.10.006

[35] Yin, C., Luo, Z., Ni, M., Cen, K., 1998. Predicting coal ash fusion temperature with aback-propagation neural network model. *Fuel* (1998) 77, 1777–1782.